

# Electrosorption of Br and Cl on Ag(100): Experiments and Computer Simulations\*

I. Abou Hamad<sup>1,2</sup>, Th. Wandlowski<sup>3</sup>, G. Brown<sup>2,4</sup>, and P.A. Rikvold<sup>1,2,5</sup>

<sup>1</sup>*Center for Materials Research and Technology and Department of Physics, Florida State University, Tallahassee, FL 32306-4350, USA*

<sup>2</sup>*School of Computational Science and Information Technology, Florida State University, Tallahassee, Florida 32306-4120, USA*

<sup>3</sup>*Institute for Thin Films and Interfaces, ISG 3, Jülich GmbH, D-52425 Jülich, Germany*

<sup>4</sup>*Center for Computational Sciences, Oak Ridge National Laboratory, Oak Ridge, TN 37831, USA*

<sup>5</sup>*Center for Stochastic Processes in Science and Engineering, Department of Physics,*

*Virginia Polytechnic Institute and State University, Blacksburg, VA 24061-0435, USA*

February 1, 2008

## Abstract

We present chronocoulometry experiments and equilibrium Monte Carlo simulations for the electrosorption of Br and Cl on Ag(100) single-crystal electrode surfaces. Two different methods are used to calculate the long-range part of the adsorbate-adsorbate interactions. The first method is a truncated-sum approach, while the second

---

\*We dedicate this paper to the memory of Michael J. Weaver. Mike's breadth, depth, and productivity, as well as his engaging personality made him an outstanding member of our community. We will miss him deeply.

is a mean-field-enhanced truncated-sum approach. To compare the two methods, the resulting isotherms are fit to experimental adsorption isotherms, assuming both a constant electrosorption valency  $\gamma$  and also a coverage-dependent  $\gamma$ . While a constant  $\gamma$  fits the Br/Ag(100) well, a coverage-dependent or potential-dependent  $\gamma$  is needed for Cl/Ag(100).

**Keywords:** Bromine electrosorption; Chlorine electrosorption; Continuous phase transition; Chronocoulometry; Lattice-gas model; Monte Carlo simulation.

## 1 Introduction

Specifically adsorbed anions strongly influence the structure and dynamics of adsorbed layers on electrode surfaces [1, 2]. Among these systems, halides electrosorbed on single-crystal metal surfaces have been extensively studied both experimentally and theoretically over the last decade. Examples of these studies include the electrosorption of Cl, Br, I, and F on low-index surfaces of Ag [3, 4, 5] employing classical electrochemical techniques [3, 5, 6, 7], (see also literature cited in ref. [5]), and structure sensitive techniques such as electroreflectance [8], *in-situ* scanning tunneling microscopy (STM) [9, 10], surface X-ray scattering (SXS) [4, 5, 11], and X-ray absorption fine structure (XAFS) [12].

Ocko, Wang, and Wandlowski [4] showed that the sharp peak observed in cyclic voltamograms of Br electrosorption on Ag(100) corresponds to a continuous phase transition in the layer of adsorbed Br. This transition separates a low-coverage disordered phase at more negative electrode potentials from a  $c(2 \times 2)$  ordered phase at more positive potentials. Moreover, in recent static and dynamic studies, Mitchell, Brown, and Rikvold [13, 14] have numerically investigated the phase ordering and disordering mechanisms in cyclic-voltammetry (CV) and sudden potential-step experiments. Using Monte Carlo simulations

of a lattice-gas model first used by Koper [15, 16], they also produced theoretical adsorption isotherms for this system that were fit to experimental adsorption isotherms. From these fits, parameters such as the electrosorption valency,  $\gamma$ , and the next-nearest neighbor interaction parameter,  $\phi_{\text{nnn}}$ , were estimated.

Less attention has been given to Cl electrosorption on Ag(100), perhaps because previous studies [3] have assumed that this system is similar to Br/Ag(100). In the present paper we compare Monte Carlo simulation results with experimental equilibrium isotherms obtained by chronocoulometry for both Cl and Br, using a lattice-gas model and two different methods for calculating the long-range part of the configuration energies.

The remainder of this paper is organized as follows. The experimental procedures and results are discussed in Sec. 2. The lattice-gas model is presented in Sec. 3. Equilibrium simulations using the two different methods of calculation are discussed in Sec. 4, and the fitting procedures and resulting parameter estimates for each system are discussed in Sec. 5. Finally, a summary and conclusions are presented in Sec. 6.

## 2 Experimental

The electrochemical measurements were performed with Ag(100) single-crystal electrodes (4 mm diameter and 4 mm thickness) using the so-called hanging meniscus technique. The silver electrodes were chemically etched in cyanide solution before each experiment until the surface appeared shiny [17] and, after careful rinsing in Milli-Q water, annealed in a hydrogen flame for about 30 s. After cooling in a stream of argon the electrode was quickly transferred into the electrochemical cell. Contact with the electrolyte was established under strict potential control, usually at values close to the potential of zero charge of 0.05 M  $\text{KClO}_4$  ( $E_{\text{pzc}} \approx -0.900$  V) [18]. The counter electrode was a platinum wire, and a saturated

calomel electrode (SCE) in a side compartment served as reference. All potentials are quoted with respect to the SCE. The temperature was  $(20 \pm 1)^\circ\text{C}$ .

The set-up and procedures for the electrochemical experiments (cyclic voltammetry, capacitance measurements, chronocoulometry) were described previously [5, 19]. We focus here only on some additional details of the chronocoulometric experiments [20]: The potential was initially held at a value  $E_i$  between  $-1.375$  V and  $-0.300$  V (25 mV interval length), up to 300 s for the lowest chloride concentrations, and then stepped to the final potential  $E_f = -1.400$  V, where chloride is completely desorbed from the electrode surface. The waiting time at  $E_i$  was chosen (in control experiments) to be always sufficient to establish adsorption equilibrium. A comprehensive account of the setup and detailed results of the SXS experiments for Ag(100)/Cl will be given elsewhere [20].

## Results of the electrochemical experiments

Figures 1(A) and 1(B) show voltammograms (CV) and capacitance (CE) curves (5 mV peak-to-peak amplitude, 18 Hz ac-frequency) for the Ag(100) electrode in 0.05 M  $\text{KClO}_4$  and 0.02 M  $\text{KCl} + 0.03$  M  $\text{KClO}_4$  as obtained after continuous cycling of the potential between  $-1.40$  V and  $-0.10$  V. The capacitance curves merge at  $E < -1.20$  V, indicating complete desorption of chloride. The onset of chloride adsorption is characterized by broad peaks in the CV and CE curves, which are labelled P1 in Fig. 1. *In-situ* SXS experiments revealed that chloride adsorbs in this potential region as a lattice gas corresponding to randomly adsorbed species on fourfold hollow sites [20]. The sharp peak P2 in Figs. 1(A) and 1(B) represents the continuous transformation of the lattice gas into an ordered  $c(2 \times 2)$  chloride adlayer [20]. This phase is stable until rather complex  $\text{AgCl}_x$ -surface compounds are being formed at more positive potentials [ $E > -0.20$  V for the system shown in Fig. 1(A)] [7, 20].

Equilibrium data on the adsorption of chloride ions at Ag(100) electrodes were obtained from chronocoulometric measurements in a gently stirred solution. Figure 1(A) shows selected charge density curves for KCl in  $(0.05 - x)$  M  $\text{KClO}_4 + x$  M KCl. Adsorption of chloride causes a positive charge to flow to the metal side of the interface. This is accompanied by a negative shift of the potential of zero charge. Phenomenologically, the charge density vs. potential curves as measured in the presence of chloride concentrations  $C_{\text{Cl}} > 10^{-3}$  M are composed of two segments. The region of low charge densities corresponds to the potential range of the broad features in the CV and CE curves. The second one appears at a potential just positive of the adlayer phase transition at P2, corresponding to charge densities between 35 and 40  $\mu\text{C cm}^{-2}$ . It is characterized by an initial increase of  $\delta q^{\text{M}}/\delta E$ . Subsequently the slope decreases and seems to become less dependent on the chloride concentration for  $C_{\text{Cl}} > 10^{-3}$  M at the most positive potentials studied.

The corresponding Gibbs surface excess has been calculated at constant potential (see Fig. 2) and constant charge (not shown, c.f. [20]), using the approach of Stolberg and Lipkowski [5, 20, 21]. The surface excess increases in the potential region of disordered chloride and at constant concentration monotonously with potential. At  $C_{\text{Cl}} > 10^{-3}$  M one observes in the potential region of the sharp volumetric peak P2 a distinct increase in slope ( $\Gamma \sim 6 \times 10^{-10}$  mol  $\text{cm}^{-2}$ ). At the most positive potentials experimentally accessible, the surface excess levels off and approaches a chloride-concentration independent limit of  $\Gamma_{\text{m}} = 10.2 \times 10^{-10}$  mol  $\text{cm}^{-2}$ . This chronocoulometric result is close to  $9.94 \times 10^{-10}$  mol  $\text{cm}^{-2}$  expected for a complete c(2 × 2) chloride adlayer, and is well supported by *in-situ* SXS experiments employing the so-called interference scattering technique [20].

The electrosorption valency, as determined from a plot of the charge density vs. surface excess at constant potential for the Ag(100)/Cl system is shown as an inset in Fig. 2. Using this method, the electrosorption valency is found to be potential dependent, decreases with

increasing potential, and approaches -0.45 at -0.40 V. This value is larger than the result for Ag(100)/Br ( $\gamma \sim -0.80$ ) [5, 13] (see also discussion in Sec. 5), indicating the stronger ionic character of adsorbed chloride, in comparison to bromide on silver.

### 3 Lattice-gas Model

The model used for both the Br and Cl systems is a lattice-gas model similar to that used by Koper [15, 16] and Mitchell *et al.* [13, 14]. In this model the Br or Cl ions adsorb at the four-fold hollow sites of the Ag(100) surface, as shown in Fig. 3. The model is defined by the grand-canonical effective Hamiltonian

$$\mathcal{H} = - \sum_{i < j} \phi_{ij} c_i c_j - \bar{\mu} \sum_{i=1}^{L^2} c_i \quad (1)$$

where  $\sum_{i < j}$  is a sum over all pairs of sites,  $\phi_{ij}$  are the lateral interaction energies between particles on the  $i$ th and  $j$ th sites measured in meV/pair, and  $\bar{\mu}$  is the electrochemical potential measured in meV/atom. Here the local occupation variables  $c_i$  can take the values 0 or 1, depending on whether site  $i$  is occupied by an ion (1) or solvated (0).

The simulations were performed on an  $L \times L$  square lattice, using periodic boundary conditions to reduce finite-size effects. The interaction constants  $\phi_{ij}$  between ions on sites  $i$  and  $j$  a distance  $r_{ij}$  apart (measured in Ag(100) lattice spacing units,  $a = 2.889$  Å [4]) are given by

$$\phi_{ij} = \begin{cases} -\infty & r_{ij} = 1 \\ \frac{2^{3/2} \phi_{\text{nnn}}}{r_{ij}^3} & r_{ij} \geq \sqrt{2} \end{cases} \quad (2)$$

where the infinite value for  $r_{ij} = 1$  indicates nearest-neighbor exclusion, the interaction for large  $r_{ij}$  is most likely a combination of dipole-dipole and surface-mediated elastic interactions, and negative values of  $\phi_{ij}$  denote repulsion. The previous studies by Koper [15, 16] have shown that large but finite nearest-neighbor repulsion has only minor effects on the

coverage isotherms. Consequently, we have chosen a simplified model with nearest-neighbor exclusion.

In the weak-solution approximation, the electrochemical potential  $\bar{\mu}$  is related to the bulk ionic concentration  $C$  and the electrode potential  $E$  (measured in mV) as

$$\bar{\mu} = \bar{\mu}_0 + k_B T \ln \frac{C}{C_0} - e\gamma E \quad (3)$$

where  $\bar{\mu}_0$  is an arbitrary constant,  $C_0$  is a reference concentration (here taken to be 1 mM),  $e$  is the elementary charge unit,  $\gamma$  is the electrosorption valency [22], and  $\bar{\mu}$  has the sign convention that  $\bar{\mu} > 0$  favors adsorption.

The anion coverage is defined as

$$\theta = N^{-1} \sum_{i=1}^N c_i, \quad (4)$$

where  $N = L^2$  is the total number of lattice sites. The coverage can be experimentally obtained by standard electrochemical methods as well as from the integer-order peaks in surface X-ray scattering (SXS) data [4, 20].

To compute the isotherms  $\theta(\bar{\mu})$  or  $\theta(E)$ , the change in energy must be calculated before each attempted Monte Carlo move. This requires evaluation of the interaction sum in Eq. (1), which is computationally intensive even for modest system sizes. In the next section we compare a direct summation approach with a more efficient truncated summation combined with a mean-field approximation for the influence of adparticle pairs at large separations.

## 4 Monte Carlo Methods

The Monte Carlo simulation proceeds as follows. On a square lattice with  $L = 64$  and periodic boundary conditions we randomly select a lattice site,  $i$ , and attempt to change the occupation variable ( $c_i = 1 \rightarrow c_i = 0$  or  $c_i = 0 \rightarrow c_i = 1$ ). The energy difference,

$\Delta\mathcal{H}$ , between the initial state of the system and the proposed state is then calculated using Eq. (1). We use the Metropolis acceptance probability [23]

$$\mathcal{R} = \min \left[ 1, \exp \left( -\frac{\Delta\mathcal{H}}{k_{\text{B}}T} \right) \right] \quad (5)$$

for accepting the new trial configuration as the next configuration in the Monte Carlo sequence.

Since the value of  $\Delta\mathcal{H}$  determines  $\mathcal{R}$  in Eq. (5), the approximations made to calculate the large- $r_{ij}$  contributions to the pair sum in Eq. (1) are important. In our computations, we used two different methods to calculate  $\Delta\mathcal{H}$ . The first was a direct-summation-plus-truncation method previously used by Mitchell *et al.* [13, 14]. In the second method, which we introduce here, we include the exact contribution of fewer sites on the surface, using a mean-field approximation to calculate the contribution from all the sites at larger distances.

## 4.1 Direct summation

The first method involves calculating the contribution of the sites that are less than or equal to five lattice spacings away from the site of interest. Since nearest-neighbor adsorption is prohibited, the acceptance probability vanishes for any move that would bring two particles into nearest-neighbor positions. In addition to the four nearest-neighbor sites, there are a total of 76 sites such that  $1 < r_{ij} \leq 5$ . These are divided between 12 different distance classes as shown in Fig. 4. This summation provides approximately 87% of the total energy due to the long-range interactions [14].

This method of approximation proved to be acceptable for simulating Br adsorption on Ag(100) [13, 14] as it produced values for the electrosorption valency  $\gamma$  that are in good agreement with experimental data. On the other hand, because of its computationally



intensive nature, this method of calculating  $\Delta\mathcal{H}$  made it harder for dynamic simulations to achieve CV scan rates within the experimental range [14].

## 4.2 Mean-field-enhanced method

The method of calculating  $\Delta\mathcal{H}$  can be modified from the previous one so that, without reducing the accuracy of the calculation, the cutoff radius is reduced from five to three lattice constants. This decreases the number of sites beyond nearest neighbors that are included in the summation from 76 to 24, as shown in Fig. 4.

This modification includes a mean-field approximation to estimate the interaction energy contribution from those particles that are farther than three lattice constants from the site in question. Consequently, the change in energy associated with desorbing from the surface a particle at lattice site  $i$  is

$$\Delta\mathcal{H}_i = 2^{3/2}\phi_{\text{nm}} \left[ \sum_{1 < r_{ij} \leq 3} \frac{c_j}{r_{ij}^3} + \theta \left( \Sigma_\infty - \sum_{1 \leq r_{ij} \leq 3} \frac{1}{r_{ij}^3} \right) \right] \quad (6)$$

which is both more efficient and more accurate than calculating the exact energy contributions out to  $r_{ij} = 5$ . Here  $\Sigma_\infty = \sum_{r=1}^{\infty} 1/r^3$  is a Zucker sum over the sites of a square lattice of unit lattice constant [15], and the quantity in the parenthesis is a constant, independent of the adsorbate configuration. It can easily be calculated to arbitrary numerical precision. The energy change upon adsorption at a previously empty site  $i$  with four empty nearest-neighbor sites is the negative of the result in Eq. (6).

This modification of the calculation of the energy changes for the Monte Carlo steps makes the program run more than twice as fast as when using the method described in Sec. 4.1 and used in Refs. [13, 14]. It is consequently better suited for dynamical simulations [24].

The results of the calculations performed with this method are similar to those using exact summation for  $r \leq 5$ . At higher coverages, the numerical effect of introducing the mean-field approximation is more pronounced, as expected. We note that this method is successful because the interactions in our model are repulsive, which ensures that the spatial distribution of adparticles is approximately uniform on large length scales. For systems with attractive interactions more sophisticated methods to calculate the contributions from the long-range interactions, such as the Fast Fourier Transform or Fast Multipole Method [25], would be needed.

### 4.3 Comparison

A comparison of the calculated coverage as a function of the electrochemical potential, obtained with both mean-field and non-mean-field methods for different cutoff radii, is shown in Fig. 5. The mean-field enhancement makes a significant contribution to the adsorption isotherms for both cutoff lengths. However, when the mean-field enhancement is used, increasing the cutoff radius beyond three does not significantly improve the results. Tests with even smaller cutoff radii revealed that three is an optimal choice to increase the computational speed with only a minimal loss of accuracy.

## 5 Parameter Estimation

To estimate the parameters in the lattice-gas model,  $\phi_{\text{nnn}}$  and  $\gamma$ , we performed standard equilibrium MC simulations [23] with  $\Delta\mathcal{H}$  calculated by the mean-field-enhanced method at room temperature ( $k_{\text{B}}T = 25$  meV or  $T \approx 290$  K) to obtain  $\theta(\bar{\mu})$  for different parameter values. These simulated isotherms were then compared with the experimental chronocoulometry data using two fitting procedures. The first procedure assumed a constant

electrosorption valency  $\gamma$ , while the second assumed a coverage-dependent  $\gamma(\theta)$ . The experimental coverage data for Br/Ag(100) [5], which were also used in Refs. [13, 14], were provided to the authors of those papers by J.X. Wang.

## 5.1 Constant $\gamma$

To extract the values of  $\gamma$  and  $\phi_{\text{nnn}}$  that would best fit the experimental data, we used a least-squares fitting procedure that minimizes  $\chi^2$  with respect to three fitting parameters for Cl and Br electrosorbed on Ag(100) [14],

$$\chi^2(\phi_{\text{nnn}}, \gamma, \bar{\mu}_0) = \sum_{k=1}^{N_{\text{conc}}} \sum_{l=1}^{l_{\text{max}}(k)} [\theta^{\text{sim}}(E_l^k; \bar{\mu}_0, \gamma, \phi_{\text{nnn}}; C_k) - \theta^{\text{exp}}(E_l^k; C_k)]^2 \quad (7)$$

where  $\theta^{\text{sim}}$  and  $\theta^{\text{exp}}$  are the simulated and experimental coverage values respectively,  $k$  is the concentration index,  $N_{\text{conc}}$  is the number of different concentrations used in a fit, and  $l$  is the point index of the experimental data points.

This fitting procedure, which provides good fits for Br/Ag(100) in Refs. [13, 14] (see also Table 1) does not give satisfactory fits for Cl/Ag(100). The assumption that the electrosorption valency  $\gamma$  is independent of the coverage is consistent with the Br results, but appears to be invalid for the Cl system.

## 5.2 $\theta$ dependent $\gamma$

Since a coverage independent  $\gamma$  does not appear to be a valid assumption for Cl/Ag(100), we assume that  $\gamma$  depends linearly on the coverage as

$$\gamma(\theta) = \gamma_0 + \gamma_1 \theta \quad (8)$$

This adds to the model a fourth parameter,  $\gamma_1$ , that must be determined by comparison to the experimental results. The  $\theta$ -dependent  $\gamma$  is allowed to vary in the interval  $[-1, 0]$ , which

limits the values that  $\gamma_0$  and  $\gamma_1$  can assume according to Eq. (8). The range of variation for  $\gamma_0$  is  $[-1, 0]$ , while it is  $[-2, 0]$  for  $\gamma_1$  since the latter is multiplied by  $\theta$ , which can assume a maximum value of 0.5. As determined by  $\chi^2$  [Eq. (7)], the inclusion of a coverage-dependent electrosorption valency improves the fits to the adsorption isotherms, shown in Fig. 6. It also gives reasonable values for  $\gamma$  and  $\phi_{\text{nmn}}$ . The resulting parameter values, based on fitting Cl and Br simulations to the experimental isotherms, are shown in Tables 1 and 2, respectively.

The tables include values for the fitting parameters,  $\gamma_c$  for the constant  $\gamma$  fits and  $\gamma_0$  and  $\gamma_1$  for the coverage-dependent fits. Moreover they include values for  $\phi_{\text{nmn}}$  and  $\chi^2$  per degree of freedom,  $\hat{\chi}^2$ , for all the fits. Fitting to the experimental data was performed both for the truncated-sum Monte Carlo isotherms and for the mean-field-enhanced isotherms. For each of these simulated isotherms we performed three kinds of fits. First, the numerical isotherms were fit to a single set of experimental data with a certain halide ion concentration (columns 3-8 in Tables 1 and 2, labeled 1-fit). Second, each numerical isotherm was simultaneously fit to two experimental isotherms with ionic concentrations of 10 mM and 20 mM for Cl or 1 mM and 10 mM for Br (columns 9 and 10, labeled 2-fit). Third, numerical isotherms were fit to three experimental isotherms simultaneously with the concentrations 6, 10 and 20 mM for Cl and 0.1, 1.0, and 10.0 mM for Br (columns 11 and 12, labeled 3-fit).

In fitting two or more isotherms simultaneously, several conclusions may be drawn from the tables shown. With one exception, the values of  $\gamma_1$  in Table 1 for Br/Ag(100) are zero (i.e.,  $|\gamma_1| < 0.01$ ) or nearly zero for all of the fits. This supports the conclusion that a constant  $\gamma$  is a good approximation for that system. Moreover, the quality of the fits is enhanced by using two or more concentrations simultaneously because this utilizes a greater number of experimental data points in one fit and constrains  $\gamma$  more directly through the  $\ln(C/C_0)$  term of Eq. (3). For constant  $\gamma$  the 2-fit and 3-fit values for  $\phi_{\text{nmn}}$  and  $\gamma$  for the mean-field-enhanced method are consistent with those obtained by the non-mean-field

method. However, smaller values of  $\hat{\chi}^2$  are found for the mean-field-enhanced method than for the non-mean-field method, indicating that the mean-field-enhanced isotherms fit slightly better to the experimental data than the non-mean-field ones. Comparing the values found using the 2-fit and 3-fit methods for mean-field-enhanced isotherms, suggests  $\phi_{\text{nm}} = -21 \pm 2$  meV and  $\gamma_c = -0.71 \pm 0.01$  as reasonable estimates. These results are consistent with those obtained in Refs. [5, 13, 14].

The results for the fits to the Cl/Ag(100) experiments are given in Table 2, whose layout is the same as for Table 1. Notice that  $\gamma_1$  assumes non-zero values for most of the fits, and that – except for the fit to the 6 mM isotherm – the values of  $\hat{\chi}^2$  obtained with variable  $\gamma$  are less than those obtained with the constant- $\gamma$  fits. This supports the conclusion that, for the Cl system, a coverage-dependent  $\gamma$  should be adopted. The exception can be attributed to the fact that the 6 mM experimental data points do not cover the whole  $\theta$  range, especially in the important region near the phase transition. Consequently, we hereafter ignore the 6 mM data in estimating parameters for the Cl/Ag(100) system. This leaves the 2-fit parameter values for a  $\theta$ -dependent  $\gamma$ . The mean-field and non-mean-field parameters are similar and, as determined by  $\hat{\chi}^2$ , provide equally valid descriptions of the experiment. From this we conclude that, for Cl/Ag(100),  $\phi_{\text{nm}} = -14 \pm 2$  meV and  $\gamma = (-0.66 \pm 0.01) + (-0.68 \pm 0.01)\theta$ . While these results for  $\gamma_0$  and  $\gamma_1$  are more negative than those obtained from the charge-density curves in Sec. 2, the trends of a stronger dependence on coverage or electrode potential and a higher (less negative) overall value than for Br/Ag(100) are the same. The reasons for the quantitative difference between the estimates based on the two methods to determine the electrosorption valency are left for future study.

## 6 Conclusions

In this paper we have presented a new method for implementing the lattice-gas model for the electrosorption of halide ions on a Ag(100) surface by introducing a mean-field-enhanced method to calculate the contributions to the configuration energy of widely separated adparticle pairs. We fit adsorption isotherms obtained by Monte Carlo simulation to the experimental adsorption isotherms based on chronocoulometric data after comparing them to the results obtained using the non-mean field method.

The isotherms from both methods were fit to experimental data for both Cl and Br. It was shown that it was safe to assume a coverage-independent or potential-dependent electrosorption valency for Br on Ag(100) while a coverage-dependent electrosorption valency had to be implemented for the Cl on Ag(100).

## Acknowledgments

We thank S.J. Mitchell, J.X. Wang, and B.M. Ocko for useful discussions. P.A.R. thanks the Physics Department of Virginia Polytechnic Institute and State University for hospitality during the final stages of this work.

Supported by US National Science Foundation Grant No. DMR-9981815 and by Florida State University through the Center for Materials Research and Technology and the School of Computational Science and Information Technology.

## References

- [1] O.M. Magnussen, Chem. Rev. 102 (2002) 679.

- [2] Th. Wandlowski, in Encyclopedia of Electrochemistry, Vol. 1, M. Urbakh and E. Gileadi (Eds.), VCH-Wiley, Weinheim, 2002, p. 383.
- [3] G. Valette, A. Hamelin, R. Parsons, Zeitschrift für Physikalische Chemie, Neue Folge 113 (1978) 71.
- [4] B.M. Ocko, J.X. Wang, Th. Wandlowski, Phys. Rev. Lett. 79 (1997) 1511.
- [5] Th. Wandlowski, J.X. Wang, B.M. Ocko, J. Electroanal. Chem. 500 (2001) 418.
- [6] A. Hamelin, in Modern Aspects of Electrochemistry, Vol.16, B.E. Conway, R.E. White, J.O.M. Bockris (Eds.). Plenum Press, New York, 1987, p. 1.
- [7] B.M. Jovic, V.D. Jovic, D.M. Drazic, J. Electroanal. Chem. 399 (1995) 197.
- [8] C. Franke, G. Piazza, D.M. Kolb, Electrochim. Acta 34 (1989) 67.
- [9] G. Aloisi, A.M. Funtikov, T. Will, J. Electroanal. Chem. 370 (1994) 297.
- [10] T. Yamata, K. Ogaki, S. Okubo, Surf. Sci. 369 (1996) 321.
- [11] B.M. Ocko, O.M. Magnussen, J.X. Wang, R.R. Adzic, Th. Wandlowski, Physica B 221 (1996) 238.
- [12] O. Endo, M. Kiguchi, T. Yokoyama, M. Ito, T. Ohta, J. Electroanal. Chem. 473 (1999) 19.
- [13] S.J. Mitchell, G. Brown, P.A. Rikvold, J. Electroanal. Chem. 493 (2000) 68.
- [14] S.J. Mitchell, G. Brown, P.A. Rikvold, Surf. Sci. 471 (2001) 125.
- [15] M.T.M. Koper, J. Electroanal. Chem. 450 (1998) 189.
- [16] M.T.M. Koper, Electrochim. Acta 44 (1998) 1207.

- [17] A. Bewick, B. Thomas, J. Electroanal. Chem. 65 (1975) 911.
- [18] M.L. Foresti, M. Innocenti, R. Guidelli, J. Electroanal. Chem. 376 (1994) 8.
- [19] T. Pajkossy, Th. Wandlowski, D.M. Kolb, J. Electroanal. Chem. 414 (1996) 209.
- [20] Th. Wandlowski, B.M. Ocko, J.X. Wang, in preparation
- [21] L. Stolberg, J. Lipkowski, in Adsorption of Organic Molecules, J. Lipkowski, P.N. Ross (Eds.). VCH, New York, 1993.
- [22] K.J. Vetter, J.W. Schultze, Ber. Bunrenge. Phys. Chem. 76 (1972) 920; *ibid* 76 (1972) 927.
- [23] D.P. Landau, K. Binder, A Guide to Monte Carlo Simulations in Statistical Physics. Cambridge Univ. Press., Cambridge, 2000.
- [24] I. Abou Hamad, *et al.*, in preparation.
- [25] L.F. Greengard, The Rapid Evaluation of Potential Fields in Particle Systems. MIT Press, Cambridge, MA, 1988.



Table 1: Fitting parameters for Br adsorption on a Ag(100) single-crystal surface, using isotherms computed with a cutoff distance of three lattice constants, and with and without mean-field interactions included. The quantity  $\hat{\chi}^2$  is the  $\chi^2$  per degree of freedom of the fit. Here, “1-fit” means individual fits for each of the three different bulk concentrations given; “2-fit” means a single, simultaneous fit for the two bulk concentrations given; and “3-fit” means a single, simultaneous fit for the three bulk concentrations given.

		1-fit; 0.1 mM, 1 mM, 10 mM						2-fit; 1 mM, 10 mM		3-fit; 0.1mM, 1 mM 10, mM	
		mean-field			no mean-field			mean-field	no mean-field	mean-field	no mean-field
$\gamma = \text{Const.}$	$\gamma_c$	-0.51	-0.49	-0.46	-0.47	-0.46	-0.45	-0.70	-0.67	-0.73	-0.70
	$\phi_{\text{nnn}}$ (meV)	-9	-10	-10	-8	-10	-11	-22	-23	-22	-23
	$\hat{\chi}^2 \times 10^5$	0.564803	2.14327	7.34073	0.680078	2.56305	8.09803	6.89425	9.46991	7.31550	9.76821
$\gamma = \gamma_0 + \gamma_1 \theta$	$\gamma_0$	-0.54	-0.49	-0.46	-0.53	-0.46	-0.45	-0.70	-0.66	-0.72	-0.68
	$\gamma_1$	-0.01	0.00	0.00	0.02	0.00	0.00	0.00	0.04	-0.01	-0.19
	$\phi_{\text{nnn(meV)}}$	-10	-10	-10	-11	-10	-11	-22	-21	-21	-16
	$\hat{\chi}^2 \times 10^5$	0.54580	2.20281	7.54464	0.69541	2.63425	8.32297	6.98496	9.53128	7.36551	8.68241

Table 2: Fitting parameters for Cl adsorption on a Ag(100) single-crystal surface, using isotherms computed with a cutoff distance of three lattice constants, and with and without mean-field interactions included. The quantities shown and the organization of the table are the same as in Table 1.

		1-fit; 6 mM, 10 mM, 20 mM						2-fit; 10 mM, 20 mM		3-fit; 6 mM, 10 mM, 20 mM	
		mean-field			no mean-field			mean-field	no mean-field	mean-field	no mean-field
$\gamma = \text{Const.}$	$\gamma_c$	-0.29	-0.35	-0.40	-0.28	-0.35	-0.46	-0.57	-0.54	-0.44	-0.44
	$\phi_{\text{nnn}}$ (meV)	-4	-6	-8	-4	-7	-14	-19	-20	-12	-14
	$\hat{\chi}^2 \times 10^5$	4.06844	5.05880	11.2260	4.11751	4.63378	10.3544	11.8302	11.7546	13.2892	13.1223
$\gamma = \gamma_0 + \gamma_1\theta$	$\gamma_0$	-0.29	-0.46	-0.66	-0.28	-0.47	-0.65	-0.67	-0.65	-0.43	-0.42
	$\gamma_1$	-0.00	-0.36	-0.68	-0.00	-0.36	-0.67	-0.66	-0.70	0.02	0.04
	$\phi_{\text{nnn}}$ (meV)	-4	-7	-12	-4	-9	-14	-14	-14	-11	-12
	$\hat{\chi}^2 \times 10^5$	4.17015	3.35255	5.61327	4.22045	2.74380	4.28522	5.93654	5.41895	13.2942	13.1225

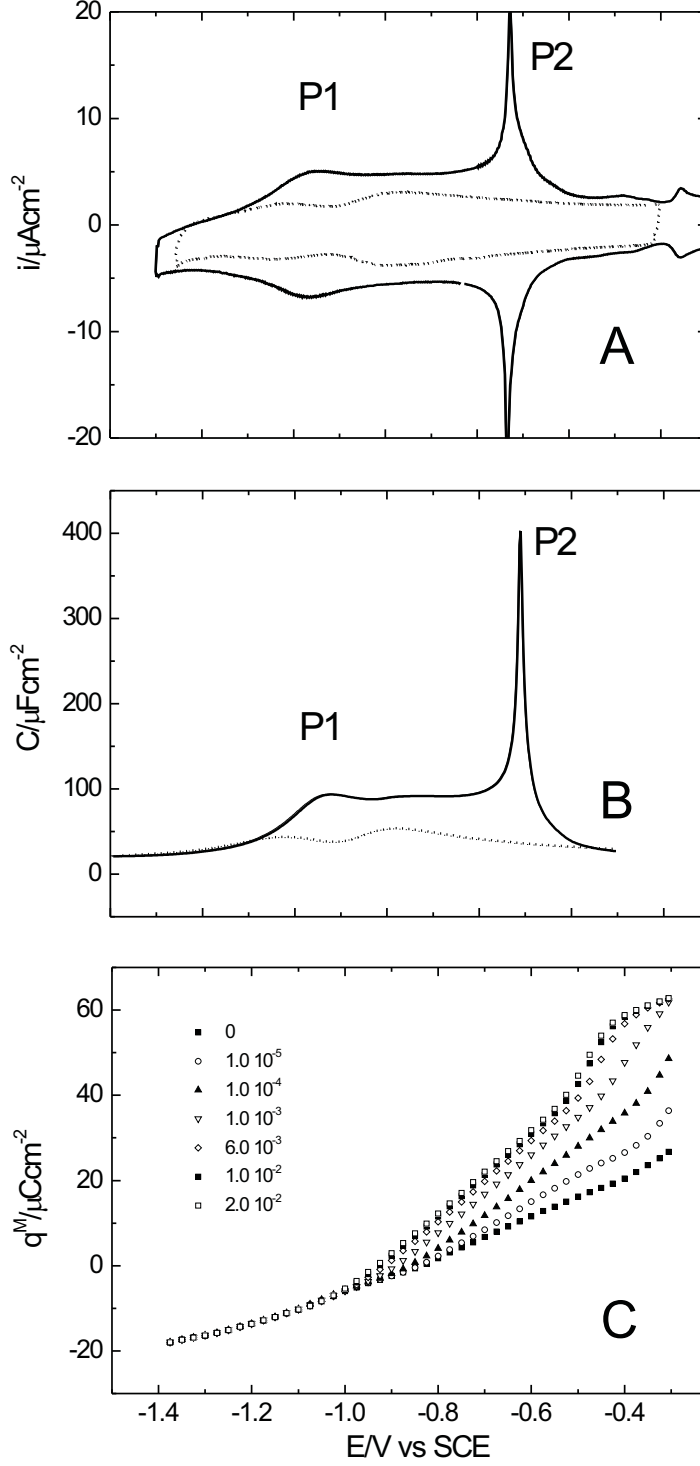


Figure 1: (A) Cyclic voltamogram ( $50 \text{ mV s}^{-1}$ ) for  $\text{Ag}(100)/(0.05 - x) \text{ M KClO}_4 + x \text{ M KCl}$ ,  $x=0$  (dotted curve) and  $x=0.02 \text{ M}$  (solid curve). (B) Capacitance vs. potential curves for the system of Fig. 1(A),  $10 \text{ mV s}^{-1}$ . (C) Charge density vs. potential curves for  $\text{Ag}(100)/(0.05 - x) \text{ M KClO}_4 + x \text{ M KCl}$  ( $x$  in M), as indicated in the figure.

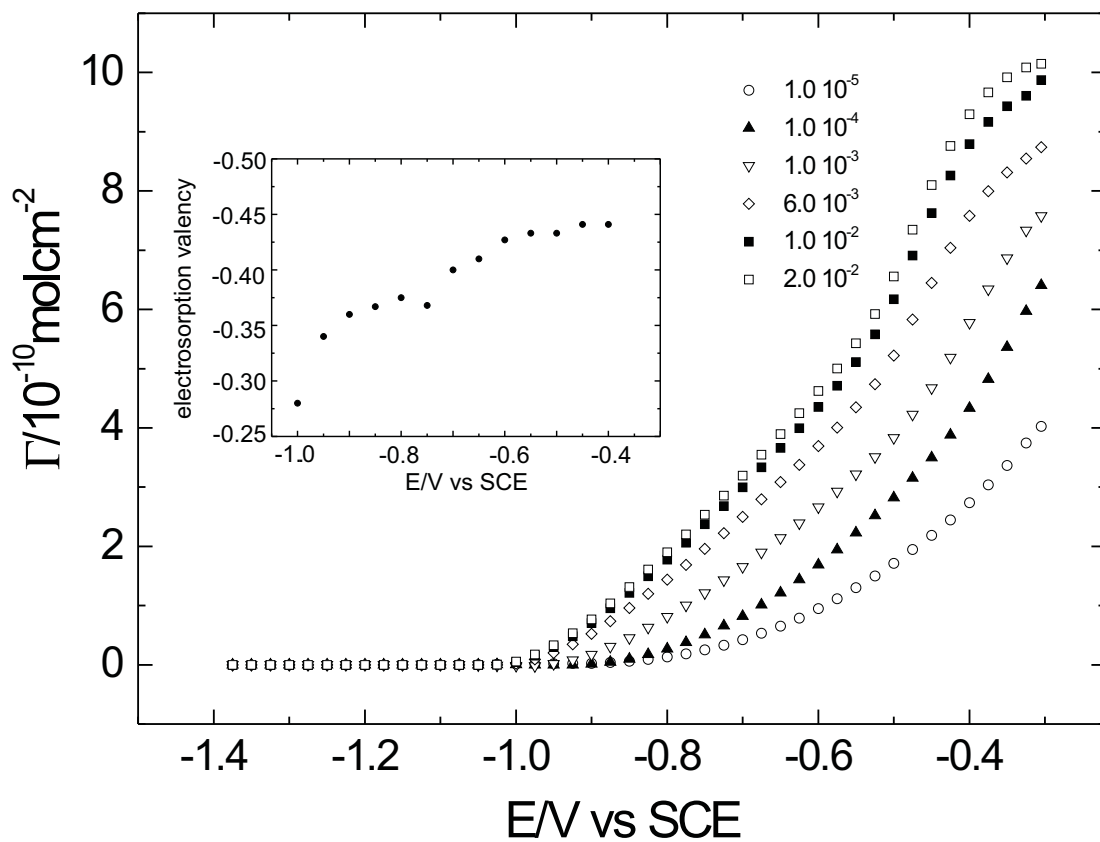


Figure 2: Plots for surface excess for  $\text{Ag}(100)/(0.05 - x) \text{ M KClO}_4 + x \text{ M KCl}$  ( $x$  in M), employing the electrode potential as the independent electrical variable for selected chloride concentrations. The inset shows the potential-dependent electrosorption valency.

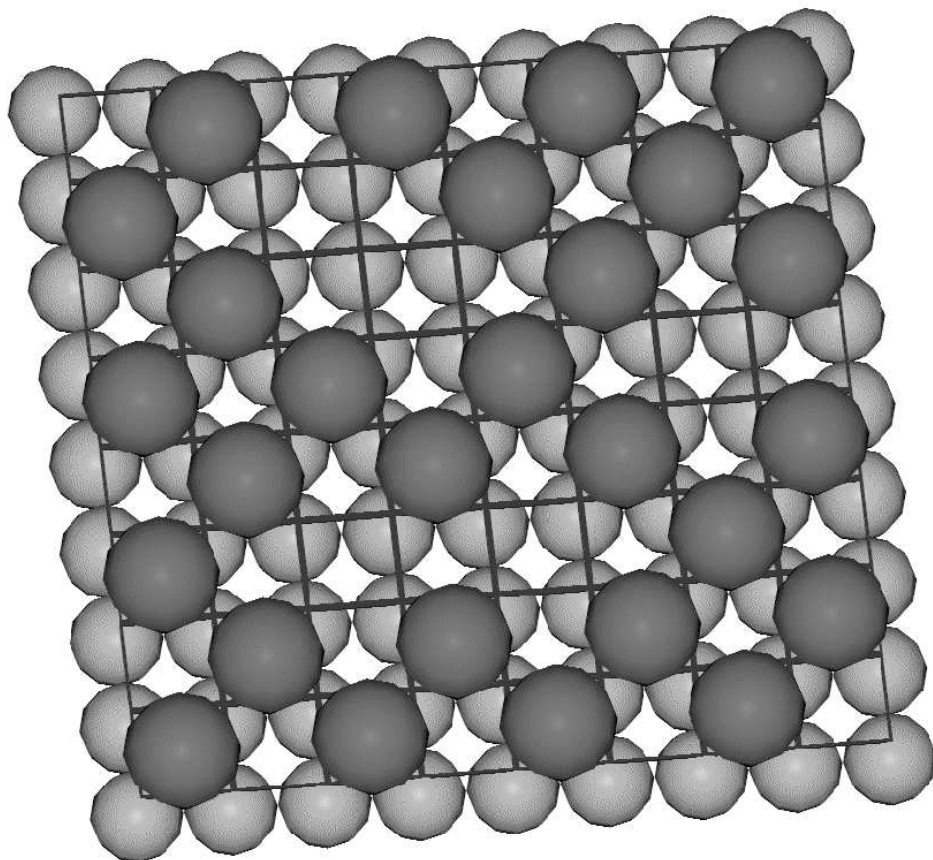


Figure 3: Br or Cl (bigger spheres) adsorbed at the 4-fold hollow sites of the (100) surface of Ag (smaller spheres). The squares of the grid frame correspond to the adsorption sites.

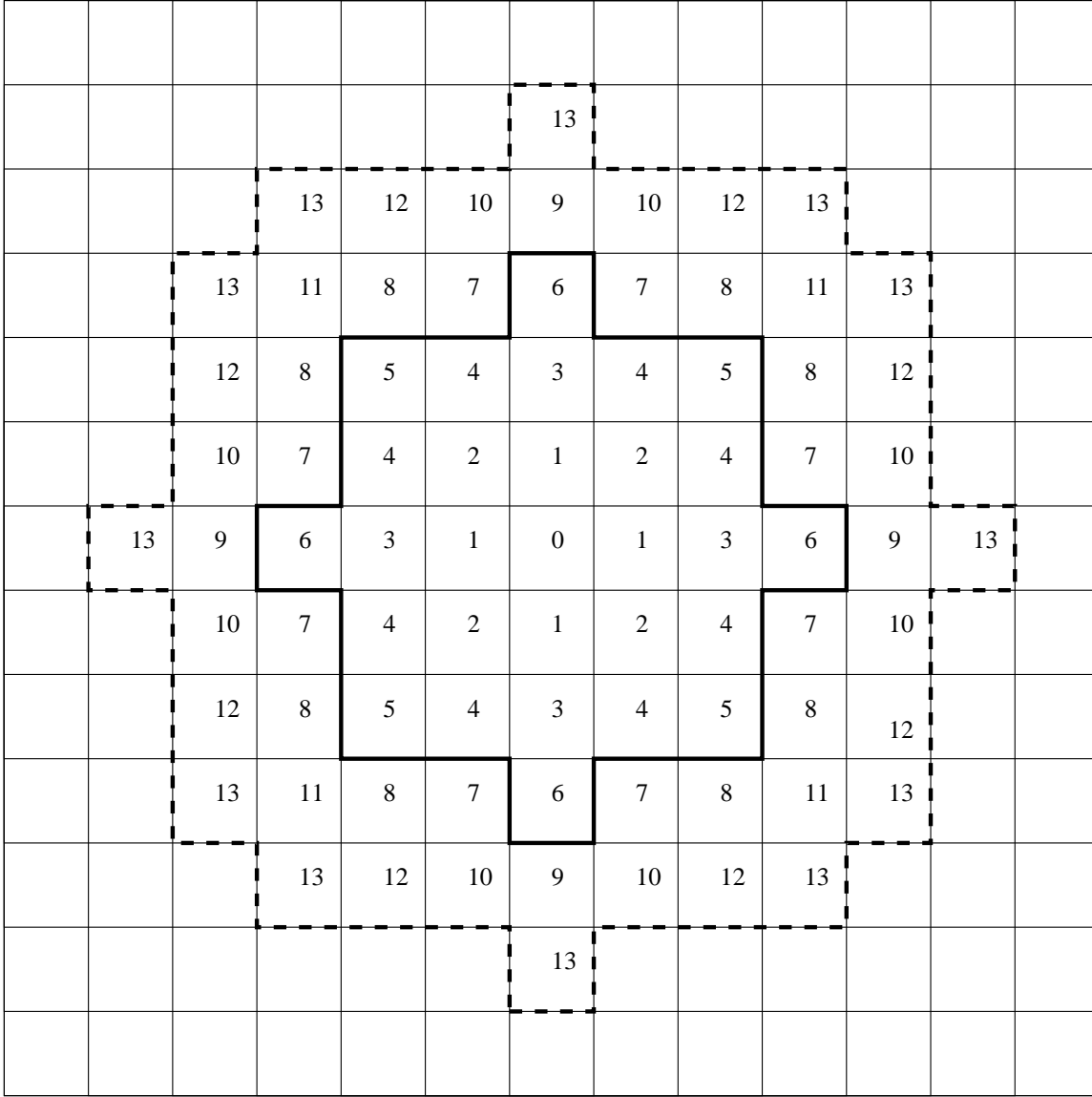


Figure 4: Sites included in the energy calculation. The dashed lines surround the 76 sites included in the direct summation for  $1 < r \leq 5$ . The heavy solid lines enclose the 24 sites included in the direct summation for  $1 < r \leq 3$ , which is used with the mean-field-enhanced method.

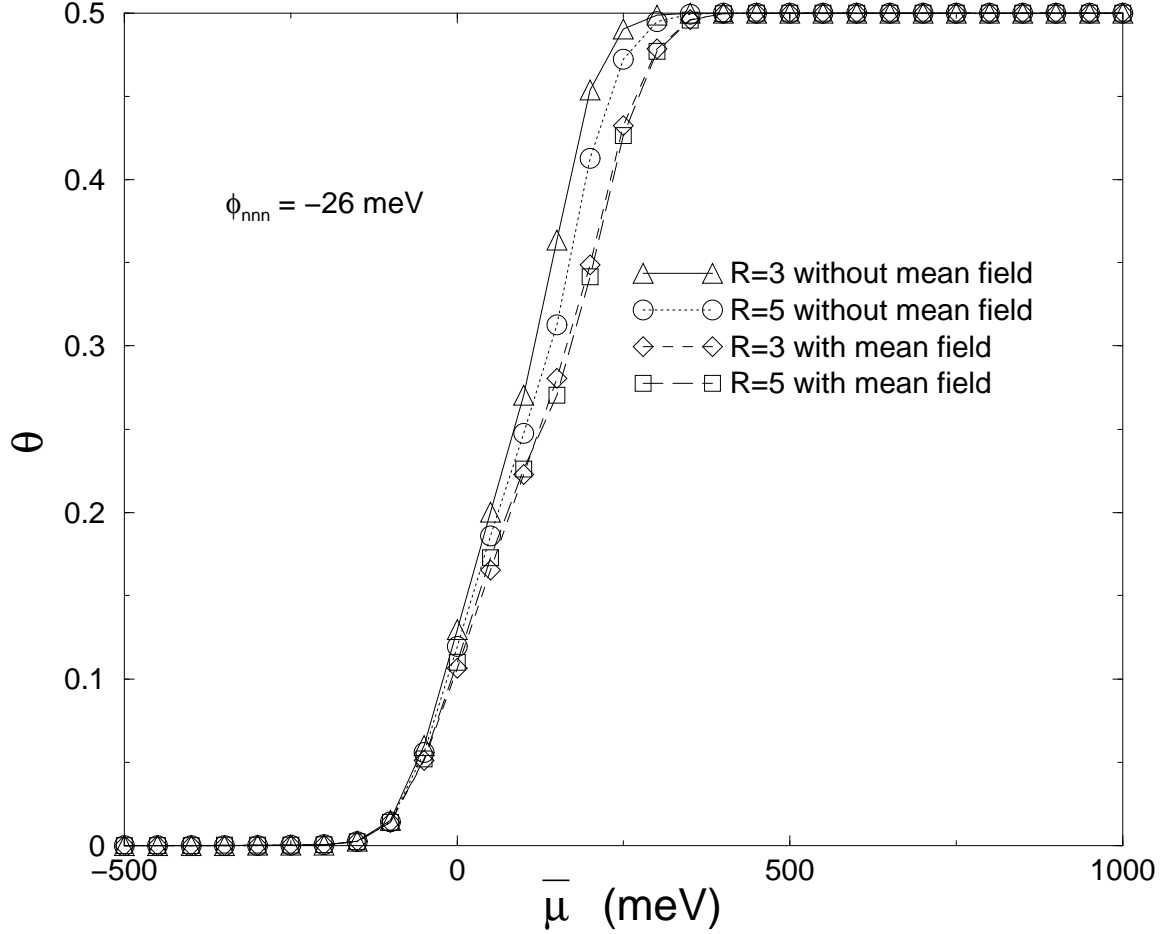


Figure 5: Simulated coverage isotherms vs. electrochemical potential, computed with different methods. Here  $R$  is the cutoff radius up to which exact summation was performed. The simulations were performed at  $T \approx 27^\circ\text{C}$  with  $\phi_{\text{nnn}} = -26$  meV. The line segments connecting the data points are included as a guide to the eye.

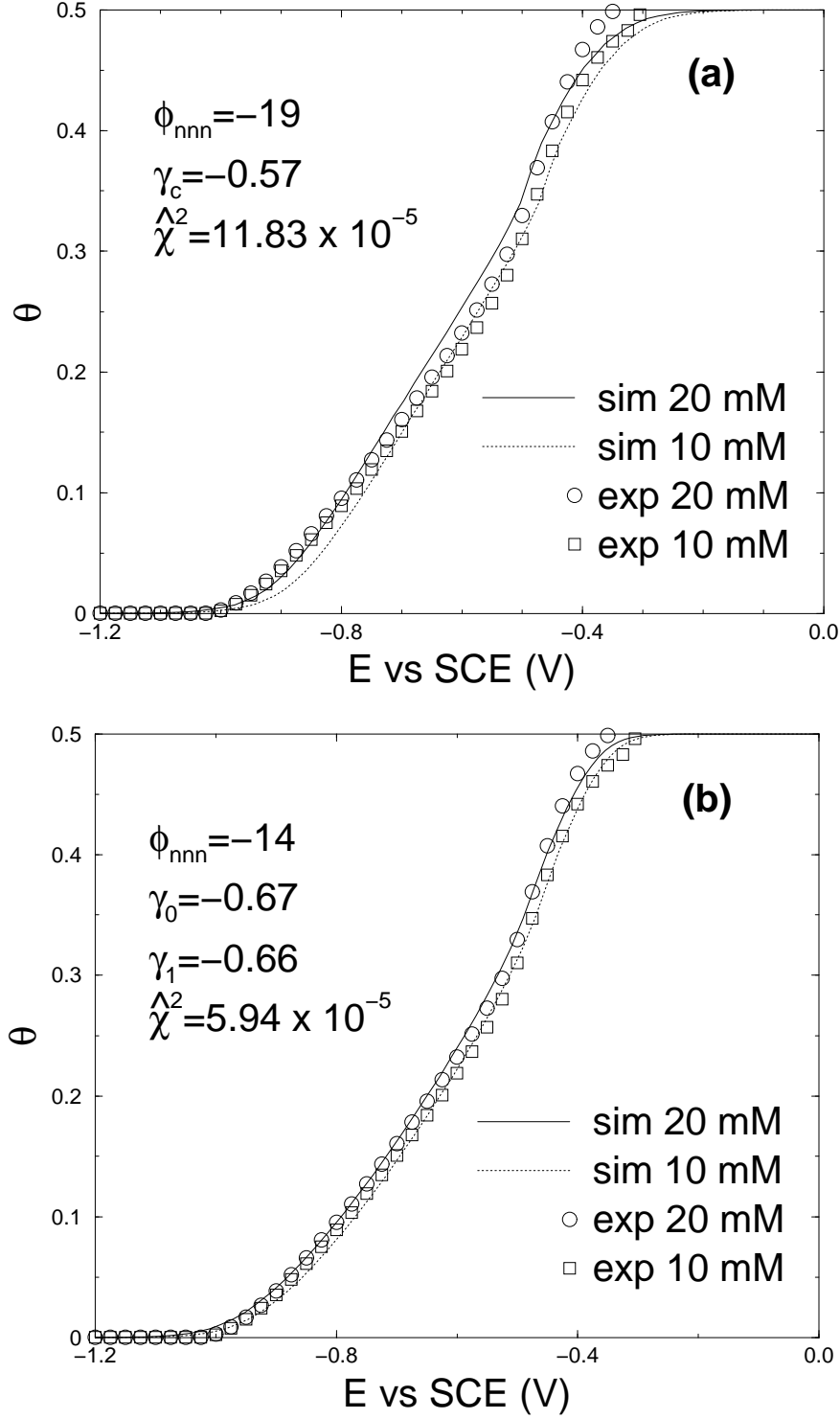


Figure 6: One simulated Cl/Ag(100) isotherm fit to two experimental isotherms with different bulk concentrations. The simulated isotherms were obtained using the mean-field-enhanced method described in Sec. 4.2. (a) Using coverage independent  $\gamma$ . (b) Using coverage-dependent  $\gamma(\theta) = \gamma_0 + \gamma_1\theta$ .